First-principles approach to calculating collision-induced absorption for H_2–H_2 pairs for the rotational, fundamental, and first overtone bands at 300K

Abordagem de primeiros princípios para cálculo absorção induzida por colisão para H_2–H_2 pares para o rotacional, fundamental e primeiras bandas de harmônicos em 300K

Fabio L. P. Costa & Gunar V. S. Mota

Absorption within the roto-translational band of H_2-H_2 is pertinent to the atmospheres of celestial bodies and outer planets characterized by elevated temperatures, fostering significant roto-vibrational excitation. A comparative analysis of the H_2-H_2 absorption spectrum with laboratory measurements at 300K reveals a consistent agreement across the entire frequency range (0 - 10000 cm^{-1}). The spectrum is primarily influenced by the quadrupole-induced dipole components ($\lambda_1\lambda_2\Lambda L$), with the most significant contributions coming from 0223 and 2023. These components, notably 0223 and 2023, play a dominant role. Beyond 3000 cm^{-1}, additional components such as quadrupole interacting ($\lambda_1\lambda_2\Lambda L$ = 2233) and others ($\lambda_1\lambda_2\Lambda L$ = 0221, 0443, 4043, 0445, and 4045) contribute to the overall absorption.

Keywords: *Collision-induced absorption; Induced-dipole moment; Molecular Hydrogen Pairs.*

A absorção na banda roto-translacional de H_2-H_2 é relevante para as atmosferas de corpos celestes e planetas externos, caracterizados por temperaturas elevadas, promovendo uma excitação roto-vibracional significativa. Uma análise comparativa do espectro de absorção H_2-H_2 com medições laboratoriais a 300K revela uma concordância consistente em toda a faixa de frequência (0 - 10000 cm^{-1}). O espectro é principalmente influenciado pelos componentes do dipolo induzido pelo quadrupolo ($\lambda_1\lambda_2\Lambda L$), com as contribuições mais significativas provenientes de 0223 e 2023. Estes componentes, especialmente 0223 e 2023, desempenham um papel dominante. Além de 3000 cm^{-1}, componentes adicionais como a interação quadrupolar ($\lambda_1\lambda_2\Lambda L$ = 2233) e outros ($\lambda_1\lambda_2\Lambda L$ = 0221, 0443, 4043, 0445 e 4045) contribuem para a absorção total.

Palavras-chave: *Absorção induzida por colisão; Momento de dipolo induzido; Pares de Hidrogênio Moleculares.*

Introdução

Collision-induced absorption (CIA) spectra were first observed in the near infrared region for gaseous oxygen by Crawford and associates in 1949[1]. The phenomenon of CIA is a characteristic across infrared frequencies, extending beyond gaseous substances[2,3], but also in many liquids and solids[4]. The spectra of dense gases exhibit distinctions from those of the same gases at low densities. With an increase in gas density, there is a potential emergence of rotovibrational and electronic bands[5], and the intensities of these spectra display a linear augmentation with the gas density. Consequently, new absorption bands manifest nonlinearly in relation to the gas density. Intermolecular interactions involving two or multiple molecules at high gas densities have been shown to produce significant collision-induced spectra. Nevertheless, dipoles induced by interaction typically exhibit lower strength compared to the permanent dipoles of molecules that are active in the infrared spectrum. Molecular symmetry is disturbed by collisions with other molecules in the gaseous phase, inducing otherwise prohibited electric dipole transitions.

The significant contribution of CIA spectra for H_2-H_2 pairs is the possibility to estimate the atmospheres of low-metallicity star as brown and white dwarfs. Because the higher predominance of the H_2 and He in the atmosphere of the cool stars[6]. CIA can become a dominant process depending on the atmosphere and pressure of the system, making it a source of opacity. According to Linsky[7], a substantial quantity of hydrogen atoms exists in their molecular state as H_2.

The atmospheric model from quantum mechanics calculation showed great advances in the description of induced dipoles, which allows an accurate in the lines shapes calculations for the reproduction of rototranslational (RT) and rotovibrational (RV) spectra for low temperatures ($T \leq 300K$)[8]. Rotovibrational combination feature line shapes which are generally very overlap and diffuse, making it difficult to identify the individual lines in the anisotropic interactions of intermolecular system[9]. Nevertheless, computations relying on the isotropic potential approximation delineate the distinct contributions to opacity, subsequently aggregating them across all permissible dipoles. For example, in Jupiter, the opacity in the atmosphere is almost entirely due to the collision-induced dipoles of H_2–H_2 and H_2–He pairs[5], in the far infrared. Three mechanisms are predominant in the formation of collisionally-induced-dipole moments in collisional pairs: 1) the induction by overlap, 2) the dispersion forces, and 3) polarization by the static multipole field.

Several models for CIA calculation have been implemented, but a special attention to the Borysow´s model[6] which allowed correction in the classical multipole models (fairly accurate) and the utilization of quantum chemical methodologies, adept at providing precise descriptions for weak van der Waals calculations, is employed.. Another problem is related at the exchange contribution, which becomes large at short distances and the perturbation theory fails to adequately solve this problem. Hence, a viable approach to address this issue is to consider the H_2-H_2 complex as a supermolecule within a self-consistent field (SCF) framework and the excitations by the configuration-interaction (CI) calculations (It is suitable for addressing the long-range effects). CIA effects are greater for low stars effective temperature, where it presents a great abundance of molecular hydrogen and a small numerical density of free electrons. In systems where gravity is high, the density is high in the atmosphere and therefore a large number density of H_2-H_2 pairs. In both cases we have low metallicity. Based on these characteristics for a system, we started the calculations with low metallicity dwarf star models.

The aim of this research is to enhance the precision of quantum mechanics calculations utilized in the determining Collision-Induced Absorption (CIA) spectra from the Fortran program codes employed in this study, and to compare with opacity values obtained from experimental data available on HITRAN database[10].

Methodology

All calculations for the H_2-H_2 pair based on first principles has as input the equations to generate the CIA spectra. When determining the induced dipole moment, the collisional complex is established through the combination of two H2 molecules, treated as a singular entity.

The first step of the calculations provides information about the rotovibrational energies of the dimer energies. It is important that first principal calculation use an isotropic potential approximation (IPA) since the experimental data for the rotovibrational lines are usually very diffuse and with overlapping. The opacity contribution can be computed for each individual element and subsequently aggregated across all permissible dipoles, facilitating a comparison with experimental data.

The expression of the induced dipole moment is presented through both its spherical components and the Cartesian components of the dipole moment (μ_x, μ_y, and μ_z) are obtained according to eq. (1).

$$\mu_{\pm 1} = \mp\frac{1}{\sqrt{2}}\left(\mu_x \pm i\mu_y\right),\ \mu_0 = \mu_z \tag{1}$$

The dipole spherical-tensor coefficients $A_{\lambda_1\lambda_2\Lambda L}$ are computed according to [11],

$$\mu^{\nu} = \frac{(4\pi)^{\frac{3}{2}}}{3^{\frac{1}{2}}}\sum A_{\lambda_1\lambda_2\Lambda L}(R,r_1,r_2)\,Y_{\lambda_1 m_1}(\Omega_1)Y_{\lambda_2 m_2}(\Omega_2)Y_{LM}(\Omega) \times \langle\lambda_1\lambda_2 m_1 m_2|\Lambda\mathrm{M}\rangle\langle\Lambda L\mathrm{m}(\mathrm{M}-m)|1\mathrm{M}\rangle \tag{2}$$

where $Y_{lm_l}(\Omega)$ are spherical harmonics, Ω_1 and Ω_2 are the orientation angles of two molecules and, Ω represents the orientation angles of the intermolecular vector R, where the sum runs over all possible values of λ_1, λ_2, m_1, m_2, Λ and m. M = 1, 0, or −1, corresponding to the dipole components and the quantities $\langle\lambda_1\lambda_2 m_1 m_2|\Lambda\mathrm{M}\rangle$ and $\langle\Lambda L\mathrm{m}(\mathrm{M}-m)|1\mathrm{M}\rangle$ are Clebsch-Gordan coefficients. For H_2–H_2, the mechanism of long-range dipole induced that contribute to the A coefficients operate within a quadrupolar field, hexadecapolar field, dispersion, and Back-induction. The Clebsch-Gordan coefficients can be rewrite by $\sum_{M m_n m_n M_\lambda} C(\lambda_1\lambda_2\Lambda; m_1 m_2 M_\Lambda) \times C(\Lambda\mathrm{L}1; M_\Lambda M_\upsilon)$[12].

For comparisons of measured spectra of diatomic molecules, collision-induced absorption spectra are dependent on the angular frequency ω and temperature T which is related to the absorption coefficient (α) by

$$\alpha(\omega,\mathrm{T}) = 2\pi(6\hbar c)^{-1}N_a\rho^2\omega\left(1-e^{-\frac{\hbar\omega}{\kappa\mathrm{T}}}\right)Vg(\omega,\mathrm{T}) \tag{3}$$

here, *Na* is Avogadro´s number, ρ the number density of the gas in amagat units, k if the Boltzmann´s constant. The spectral function (g(ω,T)) and volume (V) are given by the sum over all optical transitions,

$$Vg(\omega,\mathrm{T}) = \sum_{s,s'}P_s\sum_{t,t'}VP_t(4\pi\epsilon_0)^{-1}\left|\langle t|B_{s,s'}|t'\rangle\right|^2\delta(\omega_{s,s'}+\omega_{t,t'}-\omega) \tag{4}$$

where, $s = \{\upsilon_1\upsilon_2 j_1 j_2\}$ represents the initial rotovibrational states of molecules 1 and 2; P_s and P_t represent the population probabilities, which are dependent on temperature, for both the molecular and translational states; t is the translational state of the collisional pair; Dirac's δ function conserves energy, with $\omega_{s,s'}$ given by Eq. (3); and the dipole transition element is calculated according to β-functions,

$$B^{s,s'}_{\lambda_1\lambda_2\Lambda L}(R) = \langle\upsilon_1 j_1\upsilon_2 j_2|B_{\lambda_1\lambda_2\Lambda L}(x_1,x_2,R)|\upsilon_1' j_1'\upsilon_2' j_2'\rangle \tag{5}$$

where, $B_{\lambda_1\lambda_2\Lambda L}(x_1,x_2,R)$ are analytical function obtained by 2D-dimensional polynomials of 3rd order, with $x_i = r_i - \langle r\rangle$ for i = 1,2, with mean bond distance for zero-point vibration of $\langle r\rangle = 1.449$ bohr[5]. The molecular pair's radial rotovibrational matrix elements are denoted by the $|\upsilon_1 j_1\upsilon_2 j_2\rangle$.

The spectral function can be reformulated based on Clebsch-Gordan coefficients., as

$$g(\omega,\mathrm{T}) = \sum_{\lambda_1\lambda_2\Lambda L}\sum_{s,s'}(2j_1+1)P_1C(j_1\lambda_1 j_1';000)^2 \times (2j_1+1)P_2C(j_2\lambda_2 j_2';000)^2 \times G_{\lambda_1\lambda_2\Lambda L}(\omega-\omega_{s,s'},\mathrm{T}) \tag{6}$$

where, G functions provide an individual line profiles accord to

$$G_{\lambda_1\lambda_2\Lambda L}(\omega-\omega_{s,s'},\mathrm{T}) = \lambda_0^3\hbar\sum_{l,l'}(2l-1)C(lLl';000)^2\omega(ll' j_1 j_1' j_2 j_2') \times\int_0^\infty e^{-\frac{E_t}{\kappa\mathrm{T}}}dE_t\left|\langle t|B^{s,s'}_{\lambda_1\lambda_2\Lambda L}(R)|t'\rangle\right|^2 \tag{7}$$

The frequency shift relative the lines center is represented by $\omega - \omega_{s,s'}$ and the energy conservation is $h(\omega - \omega_{s,s'}) = E_{t'} - E_t$. Thus, Fortran program computes the translational dipole matrix elements by $\langle E_t l | B^{s,s'}_{\lambda_1\lambda_2\Lambda L}(R) | E_{t'} t' \rangle$ required in the individual profiles. A subsequent Fortran program is employed to calculate the "absorption line." It subsequently computes the individual line profile, represented by the integral in Equation (7), and generates files containing these profiles on a frequency and temperature grid. These profiles must then be aggregated across all significant line profiles. The matrix elements of collision-induced translational radial dipole are computed across a frequency range from 0 to 20,000 cm^{-1}, and the program calculates the individual line profile for each frequency. The Fortran codes subsequently generate files containing these profiles on a grid of frequencies and temperatures, which must be summed over to obtain the total absorption. To obtain the matrix elements for radial transitions of induced dipole components, the dependence on the vibrational and rotational states was incorporated.

Results and Discussion

Figure 1 shows the computed absorption spectrum (solid curve) for H_2-H_2 pairs at the temperature T of 300K, and frequencies from 0 to 3000 cm^{-1}, which correspond at the rotational band. HITRAN measurements[10] (unfilled circle) is shown and presented a good agreement with calculated data. At 300K several bands of dipole forbidden are observed at frequency bands and high vibrational for the states populated of $\lambda_1\lambda_2\Lambda L$ = 0221, 2021, 0223, 2023, 2233, 0445, 4045, 0443, and 4043. The 2023, 0223, 0221, 2021, and 2233 are the terms with significant contribution to the total intensity in the rotational band. The other terms have a smaller contribution, but not least.

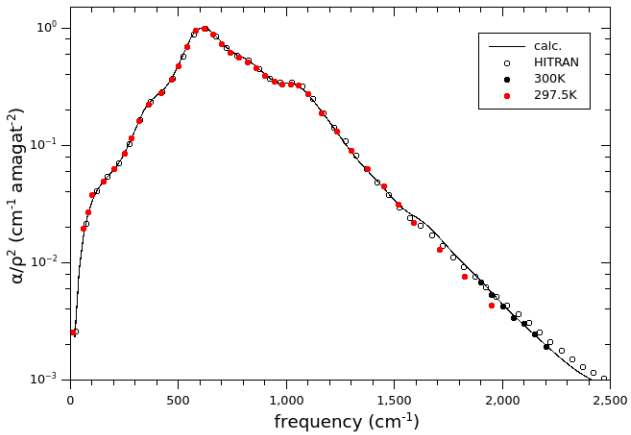

Figure 1. Rotational band of the calculated absorption spectrum (–) of pairs of molecular hydrogen in the rotational band of H2, at the temperature of 300 K, in comparison with HITRAN measurements (circle), Ref.[19] (black dots) and Ref.[21] (red dots).

When the frequencies are negligible, the argument of the exponential function can be disregarded. Nevertheless, as the excitation energies approach comparability with thermal energy, k_BT, and the exponential function argument assumes significance within the Boltzmann factor present in the equation for the absorption coefficient.

The spectral features exhibited by the rotational band can be explained through the $S_0(0)$, $S_0(1)$, $S_0(2)$ and $S_0(3)$ sharp zero phonon transitions, and $U_0(0)$ and $U_0(1)$ hexadecapolar interactions, which involve the internal degrees of freedom of molecules, and hexadecapolar induction play pivotal roles. The isotropic part of the polarizability in the hexadecapolar-induction mechanism contributes to the intensity of zero-phonon transitions such as U(J). Sidebands of phonon branches on the higher wave-number side of the zero-phonon transitions are caused by electron overlap interaction [13,14].

Fig. 2 shows an ab initio calculation (identified by solid curve) of the fundamental band at 300K, based on the new dipole used in Fortran codes and in the potential energy surface. The solid curve represents the vibrational excitation calculation, while the circle corresponds to the HITRAN data. The spectral features exhibited by the fundamental

band can be explained through the $S_1(0)$ and $S_1(1)$ sharp zero phonon transitions, and $Q_1(1)$ quadrupolar interaction.

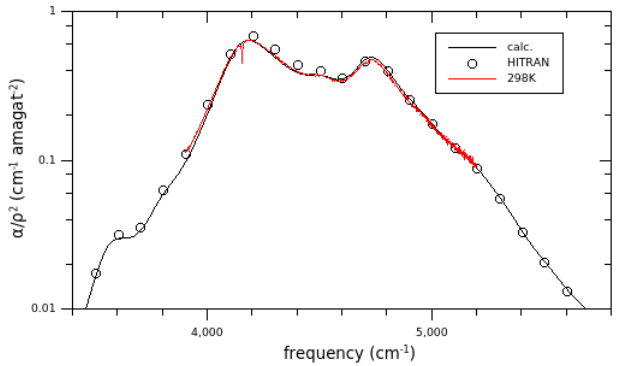

Figure 2. The comparison between the calculated H_2-H_2 spectrum (solid curve), HITRAN data (circles) and Ref.[22] (slightly noisy) for the fundamental band at 300K.

The collision induced absorption spectrum is primarily consists of dipole components denoted by $\lambda_1\lambda_2\Lambda L$ = 0001, 0221, 2021, 0223,2023,2233, 0445, 4045, 0443, and 4043. The 0001, 2023, 0223, 0221, and 2021 are the terms with largest contribution to the total intensity in the rotational band in the spectrum.

The most prominent aspect of the band is the wide Q branch that displays a double peak structure, comprising two distinct components labeled as the low and high frequency components of the Q branch, identified as Q_P (~4180 cm^{-1}) and Q_R (~4200 cm^{-1}), respectively. GUSH *et al.*[15] conducted a thorough investigation of the Q branch shape of the molecules pairs, particularly at elevated temperatures, and found that the observed profile is a composite of split Q(J) branches, which are broad and exhibit relative intensities that correspond to the population distribution of rotational levels. The observed structures can be attributed to kinetic energy interactions, which are already recognized as the cause of the main constituents, Q_P and Q_R, of the Q branch. At room temperature, the Q branch originates from the overlap of dipole moments resulting from the quadrupole-induced dipole moment. At elevated temperatures, discerning between quadrupole and overlap effects poses a challenge; hence, a uniform shape is presumed for all lines in the Q branch[16].

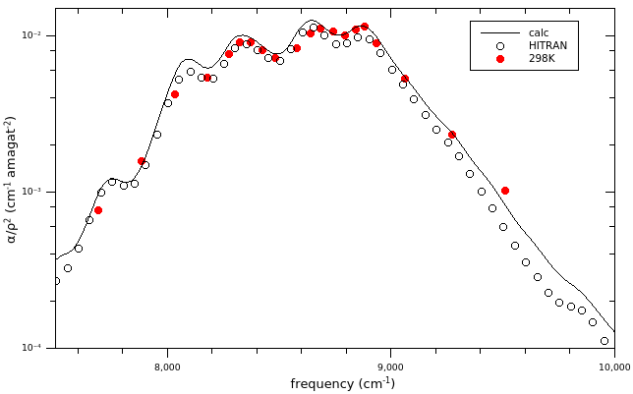

Figure 3 The comparison between the calculated H_2-H_2 spectrum (solid curve), HITRAN data (circles) and Ref.[23] (red dots) for the first overtone band at 300K.

The first overtone band at 300K extends over a frequency region from 7500 and 10000 cm^{-1}, as shown in Fig. 3 for hydrogen pairs. The ab initio calculation (solid curve) for the overtone presents an absorption spectrum composed of dipole components $\lambda_1\lambda_2\Lambda L$ = 0001, 0221, 2021, 0223,2023,2233, 0445, 4045, 0443, 4043, and 2211. The 0001, 2023, 0223, 0221, 2021, and 2233 are the terms with large contribution to the total intensity in the rotational band in the collisional spectrum. The overtones show a decrease in the dipole strength of both quadrupolar and hexadecapolar interactions. However, at high densities, no Q-branch splitting is observed, which may be mainly due to quadrupole interaction, as opposed to at low temperatures[17]. The spectral features exhibited by the first overtone band can be explained through the $S_2(0)$ and $S_2(1)$ sharp zero phonon transitions, and $Q_2(1)$ quadrupolar interaction. When a system is cooled to a helium temperature, the double transition can be observed with significant intensity. However, as the temperature increases, the transition becomes wide enough to allow for accurate identification of the individual contributions.

Due to overlap induction, the 0001 component plays a crucial role in absorption. This phenomenon arises from the distinction between a vibrating H_2 molecule and a non-vibrating one, as it undergoes periodic back-and-forth movements around its equilibrium position. Consequently,

the vibration of the H_2 molecule causes a shift in the relative positions of its atoms, thereby influencing mainly the molecular energy.

The discrepancy in the spectrum may be attributed to neglected vibrational excitation in the potential that was used. The potential used in the theoretical calculation is isotropic, meaning that it does not depend on the orientation of the atoms, but only on their separation distance. The interaction energy between two particles is modeled as the sum of a repulsive term, an attractive term, and a short-range term that accounts for steric repulsion[14].

At the time, uncertainty persisted regarding the potential influence of three-body and higher-order interactions on the measurement, or whether earlier calculations suffered from insufficient convergence to the high-order spherical dipole tensor coefficients[9]. For instance, the expansion of the components in the spherical tensor on the induced dipole surface may have been truncated prematurely, making it infeasible to include additional dipole components. On the other hand, the assessment of the far wing of the translational spectrum presents challenges owing to its weak absorption, thereby requiring the utilization of relatively elevated gas densities for the acquisition of low-noise signals. Nevertheless, as previously highlighted, elevated gas densities commonly give rise to the emergence of ternary and potentially higher-order contributions. Distinguishing these contributions from the intended purely binary ones may pose a challenge. Consequently, it is plausible that the measurement was affected by ternary and possibly higher-order contributions to an unknown degree [18–20]. While theory can compute the binary spectra, there have been no attempts to calculate ternary spectra.

Conclusion

The presented computations are grounded in novel ab initio induced dipole and potential energy surfaces for rotovibrating H2 molecules. The absorption spectra of hydrogen pairs were determined utilizing highly correlated wave functions to compute the induced-dipole moment and account for the vibrational dependencies of the isotropic part of the interaction potential.

Collision-induced spectra stemming from interactions involving three or more atoms or molecules are omitted due to inadequate comprehension, and the HITRAN collection exclusively encompasses binary spectra. The conformity between the calculated and experimental profiles demonstrates that the theory faithfully reproduces the band's structure. However, a slight systematic discrepancy is evident in the predicted intensities of single and double transitions.

The exhibited measurements showcase a noteworthy level of concordance with the theory, revealing minimal deviations. Nevertheless, any disparities noted beyond the 7000 cm^{-1} thresholds can be ascribed to the constraints inherent in a theory based on binary interactions.

Acknowledgments

Financial support for this work was provided by CNPq, Grant No. 249255/2013-8. The authors would like to express their gratitude to Professor Lothar Frornnhold for engaging discussions.

DECLARATION OF COMPETING INTEREST

The authors assert that no conflicts of interest exist with respect to the publication of this research paper.

AUTHORSHIP CONTRIBUTION STATEMENT

Dr Gunar V S Mota: Conceptualization, Investigation, Methodology, Visualization, Writing-original draft. **Dr. Fabio L P Costa**: Data curation, Writing-review editing.

References

1. Crawford, M. F.; Welsh, H. L.; Locke, J. L.; Physical Review **1949**, 75, 1607. https://doi.org/10.1103/PhysRev.75.1607.
2. Welsh, H. L.; Crawford, M. F.; MacDonald, J. C. F.; Chisholm, D. A.; Physical Review **1951**, 83, 1264. https://doi.org/10.1103/PhysRev.83.1264.
3. H. L. Welsh.; In MTP International Review of Science—Physical Chemistry, Series One, Vol. III: Spectroscopy.; Buckingham, A. D., Ramsay, D. A., Eds.; Butterworths: London, **1972**.
4. Allin, E. J.; Hare, W. F. J.; MacDonald, R. E.; Physical Review **1955**, 98, 554. https://doi.org/10.1103/PhysRev.98.554.

5. Frommhold, L.; Collision-Induced Absorption in Gases; Cambridge University Press, **1994**.

6. Zheng, C.; Borysow, A.; Astrophys J **1995**, 441, 960. https://doi.org/10.1086/175415.

7. Linsky, J. L.; Astrophys J **1969**, 156, 989. https://doi.org/10.1086/150030.

8. Meyer, W.; Borysow, A.; Frommhold, L.; Phys Rev A (Coll Park) **1989**, 40, 6931. https://doi.org/10.1103/PhysRevA.40.6931.

9. Gustafsson, M.; Frommhold, L.; Bailly, D.; Bouanich, J.-P.; Brodbeck, C.; J Chem Phys **2003**, 119, 12264. https://doi.org/10.1063/1.1625635.

10. Gordon, I. E.; Rothman, L. S.; Hargreaves, R. J.; Hashemi, R.; Karlovets, E. v; Skinner, F. M.; Conway, E. K.; Hill, C.; Kochanov, R. v; Tan, Y.; Wcisło, P.; Finenko, A. A.; Nelson, K.; Bernath, P. F.; Birk, M.; Boudon, V.; Campargue, A.; Chance, K. v; Coustenis, A.; Drouin, B. J.; Flaud, J. –M.; Gamache, R. R.; Hodges, J. T.; Jacquemart, D.; Mlawer, E. J.; Nikitin, A. v; Perevalov, V. I.; Rotger, M.; Tennyson, J.; Toon, G. C.; Tran, H.; Tyuterev, V. G.; Adkins, E. M.; Baker, A.; Barbe, A.; Canè, E.; Császár, A. G.; Dudaryonok, A.; Egorov, O.; Fleisher, A. J.; Fleurbaey, H.; Foltynowicz, A.; Furtenbacher, T.; Harrison, J. J.; Hartmann, J. –M.; Horneman, V. –M.; Huang, X.; Karman, T.; Karns, J.; Kassi, S.; Kleiner, I.; Kofman, V.; Kwabia–Tchana, F.; Lavrentieva, N. N.; Lee, T. J.; Long, D. A.; Lukashevskaya, A. A.; Lyulin, O. M.; Makhnev, V. Yu.; Matt, W.; Massie, S. T.; Melosso, M.; Mikhailenko, S. N.; Mondelain, D.; Müller, H. S. P.; Naumenko, O. v; Perrin, A.; Polyansky, O. L.; Raddaoui, E.; Raston, P. L.; Reed, Z. D.; Rey, M.; Richard, C.; Tóbiás, R.; Sadiek, I.; Schwenke, D. W.; Starikova, E.; Sung, K.; Tamassia, F.; Tashkun, S. A.; vander Auwera, J.; Vasilenko, I. A.; Vigasin, A. A.; Villanueva, G. L.; Vispoel, B.; Wagner, G.; Yachmenev, A.; Yurchenko, S. N.; J Quant Spectrosc Radiat Transf **2022**, 277, 107949. https://doi.org/https://doi.org/10.1016/j.jqsrt.2021.107949.

11. Poll, J. D.; Wolniewicz, L.; J Chem Phys **1978**, 68, 3053. https://doi.org/10.1063/1.436171.

12. Abel, M.; Frommhold, L.; Can J Phys **2013**, 91, 857–869. https://doi.org/10.1139/cjp-2012-0532.

13. Varghese, G.; Prasad, R. D. G.; Paddi Reddy, S.; Phys Rev A (Coll Park) **1987**, 35, 701. https://doi.org/10.1103/PhysRevA.35.701.

14. Li, X.; Hunt, K. L. C.; Wang, F.; Abel, M.; Frommhold, L.; Int J Spectrosc **2010**, 2010, 371201-11. https://doi.org/10.1155/2010/371201.

15. Gush, H. P.; Nanassy, A.; Welsh, H. L.; Can J Phys **1957**, 35, 712. https://doi.org/10.1139/p57-077.

16. Patch, R. W. J; Quant Spectrosc Radiat Transf **1971**, 11, 1331. https://doi.org/https://doi.org/10.1016/0022-4073(71)90003-3.

17. Watanabe, A.; Hunt, J. L.; Welsh, H. L.; Can J Phys **1971**, 49, 860. https://doi.org/10.1139/p71-102.

18. Bouanich, J. P.; Brodbeck, C.; Nguyen-Van-Thanh; Drossart, P.; J Quant Spectrosc Radiat Transf **1990**, 44, 393. https://doi.org/https://doi.org/10.1016/0022-4073(90)90120-U.

19. Bouanich, J. P.; Brodbeck, C.; Drossart, P.; Lellouch, E.; J Quant Spectrosc Radiat Transf **1989**, 42, 141. https://doi.org/https://doi.org/10.1016/0022-4073(89)90096-4.

20. Meyer, W.; Frommhold, L.; Birnbaum, G.; Phys Rev A (Coll Park) **1989**, 39, 2434. https://doi.org/10.1103/PhysRevA.39.2434.

21. Bachet, G.; Cohen, E. R.; Dore, P.; Birnbaum, G.; Can J Phys **1983**, 61, 591. https://doi.org/10.1139/p83-074.

22. Brodbeck, C.; Nguyen-Van-Thanh; Jean-Louis, A.; Bouanich, J.-P.; Frommhold, L.; Phys Rev A (Coll Park) **1994**, 50, 484. https://doi.org/10.1103/PhysRevA.50.484.

23. Hunt, J. L.; Welsh, H. L.; Can J Phys **1964**, 42, 873. https://doi.org/10.1139/p64-082.

Fabio L. P. Costa[1] & Gunar V. S. Mota[2*]

[1]Department of Chemistry, UFJ, Jataí, GO, Brazil.

[2]Institute of Exact and Natural Sciences, UFPA, Belém-PA, Brazil.

*E-mail: gunar@ufpa.br